Xiong, C., Xu, J., Wu, K., Yuan, W. (2018): Longitudinal Thin Structure of Equatorial Plasma Depletions Coincidently Observed by Swarm Constellation and all-Sky Imager. - *Journal of Geophysical Research*, *123*, 2, pp. 1593—1602.

DOI: http://doi.org/10.1002/2017JA025091

AGU PUBLICATIONS

JGR

Journal of Geophysical Research: Space Physics

RESEARCH ARTICLE
10.1002/2017JA025091

Key Points:
- The Swarm lower pair satellites, flying side-by-side separated by 1.4° in longitude, often observed EPIs showing quite different structures
- The observations from all-sky imager explained well the differences of in situ Ne measurements simultaneously observed by Swarm satellites
- For the first time both the bifurcation and merging processes were reported from one EPD example

Correspondence to:
C. Xiong,
bear@gfz-potsdam.de

Citation:
Xiong, C., Xu, J., Wu, K., & Yuan, W. (2018). Longitudinal thin structure of equatorial plasma depletions coincidently observed by *Swarm* constellation and all-sky imager. *Journal of Geophysical Research: Space Physics*, *123*, 1593–1602. https://doi.org/10.1002/2017JA025091

Received 5 DEC 2017
Accepted 28 JAN 2018
Accepted article online 5 FEB 2018
Published online 22 FEB 2018

Longitudinal Thin Structure of Equatorial Plasma Depletions Coincidently Observed by *Swarm* Constellation and all-Sky Imager

Chao Xiong[1], Jiyao Xu[2,3], Kun Wu[2,3], and Wei Yuan[2,3]

[1]GFZ German Research Centre for Geosciences, Potsdam, Germany, [2]State Key laboratory of Space Weather, National Space Science Center, Chinese Academy of Sciences, Beijing, China, [3]College of Earth Sciences, University of the Chinese Academy of Sciences, Beijing, China

Abstract The lower pair satellites of *Swarm* mission, flying side-by-side and separated by 1.4° in longitude (about 150 km), usually observed equatorial plasma depletions (EPDs) showing quite different structures, and sometime even only one satellite observed EPD. In this study, we provided 6-h continuous observations of EPDs on the night of 23–24 September 2014, from an all-sky imager located at Fuke (geographic:19.5°N,109.1°E), south of China. From the airglow images the EPDs were found with longitudinal extensions of about 50 km and all tilted from northwest to southeast direction. We further checked the in situ electron density simultaneously measured by the *Swarm* lower pair satellites and found the differences of *Swarm* in situ electron densities explained well by the longitudinally thin structure of EPDs observed from the all-sky imager. During later periods the bifurcation and merging were observed by the airglow images, and it was the first time to report both processes in the evolution of one EPD. The bifurcation was first observed at the higher-latitude part, and then observed at lower latitudes of EPD. The subbranches generated through bifurcation showed even thinner longitudinal extension of about 20–30 km, and later the subbranches started to merge with each other, forming a really complicated mesh of depleted regions.

1. Introduction

The equatorial plasma depletion (EPD) is an important space weather phenomenon at the equatorial- and low-latitude regions after sunset hours, which can cause disturbances on the transionopsheric radio wave signals. These irregularities are known to be produced via upward drift of the low-density plasma from the bottomside *F* region into the high-density topside region by the gravitational Rayleigh-Taylor instability (Kelley, 2009) and spread in a wide spatial range with scale sizes from thousands of kilometers down to meters (e.g., Hysell & Seyler, 1998; Lühr et al., 2014; Su et al., 2001). The EPD was first observed by Booker and Wells (1938), who observed the *F* region diffuse echoes from an ionosonde near Huancayo, Peru. Afterward, other techniques, such as ground-based receivers, incoherent radars, all-sky imager, rocket-born probes, and low-Earth orbital (LEO) satellites, have been widely used to investigate the EPDs' morphology, including the generation and evolution processes, spatial structures, global occurrence, and their effects on the Global Navigation Satellite System signals (Burke et al., 2004; Huang et al., 2014; Kelley et al., 1976; Kil et al., 2004; Stolle et al., 2006; Su et al., 2006; Tsunoda, 1980; Weber et al., 1978; Xiong et al., 2010; Xiong, Stolle, & Lühr, 2016).

One interesting feature of EPDs is their longitudinal extension, which has been extensively investigated by both ground-based and in situ measurements. Earlier studies, for example, Mukherjee et al. (1998) and Pimenta et al. (2003), found EPDs showing typical longitudinal extension of about 40–250 km in the all-sky imager observations. A recent study of Wu et al. (2017) showed some interesting features of EPDs, based on observations from two all-sky imagers located at south of China, Fuke (geographic:19.5°N, 109.1°E; geomagnetic: 9.5°N, 178.4°W) and Guiping (geographic: 23.8°N, 110.7°E; geomagnetic: 13.9°N, 176.8°W). The imagers often observed EPDs with planar wave-like structures, but sometime formed quite different shapes, for example, the inverted "C-shell," "C-shell," or even "I," "S," or "Y" shapes. The authors suggested that the latitudinal gradients of the zonal neutral wind, plasma zonal drift, and the ionospheric conductivity can cause the EPDs' tilt with respect to geomagnetic meridian. Similar suggestions have also been proposed by Kil et al. (2009) and Huba et al. (2009) to explain the inverted "C-shell" and "C-shell" structures

of EPDs from both observations and model simulations. Wu et al. (2017) further pointed out that the change of the background ionospheric and neutral background condition will also change the shapes of EPDs in their later development.

The in situ measurements from LEO satellite reflect only the plasma variations along the satellite track; therefore, only the LEO satellites with low elevation angles, for example, Republic of China Satellite 1 (inclination 35°) and Communications/Navigation Outage Forecasting System (inclination 13°), are suitable to investigate the longitudinal structures of EPDs. However, due to the constellation aspect, the *Swarm* mission of the European Space Agency, although with high inclination (>87°), has also provided possible opportunity for investigating the longitudinal extension of EPDs. By performing a cross-correlation analysis between the *Swarm* measured plasma density time series of EPDs, Xiong, Stolle, Lühr, Park, et al. (2016) found that the correlation between neighboring satellite measurements rapidly decreased over tenths of a degree in longitude, and with longitudinal separations larger than 0.4° (about 44 km), no significant correlation was found any more. Their results suggested that the EPDs usually have longitudinal scale of about 44 km. The EPDs reported by Wu et al. (2017) showed longitudinal extension of about 50 km from the airglow images, which is also expected to explain the difference between the in situ electron density depletions observed by the *Swarm* lower pair satellites. Therefore, in this study we provided such one example of EPD coincidently observed by the *Swarm* satellites and all-sky imager, showing well consistency between the two independent techniques.

2. Data Set

2.1. *Swarm* Constellation and In Situ Electron Density Measurements

The *Swarm* constellation is composed of three identical satellites and launched on 22 November 2013 into a near-polar orbit (87.5° inclination) with initial altitude (ALT) of about 500 km. After the maneuver, the lower pair, *Swarm* A and C, was flying side-by-side at an ALT of about 470 km, with longitudinal separation of about 1.4° (about 150 km), and the third spacecraft, *Swarm* B, orbits the Earth at about 520 km with a higher inclination. *Swarm* A and C need about 133 days for covering 24 local time (LT) hours, while *Swarm* B needs about 141 days. The plasma density data set measured by the Electric Field Instrument onboard *Swarm* is available at http://earth.esa.int/swarm. In this study we are using the Langmuir Probe-derived plasma density data with a time resolution of 2 Hz.

2.2. All-Sky Imager

The all-sky airglow imager used in this study is located at Fuke (geographic: 19.5°N, 109.1°E; geomagnetic: 9.5°N, 178.4°W), south of China. The charge-coupled device detector of the imager consists of 1,024 × 1,024 pixels with pixel depth of 16 bits and uses a 14 nm × 14 nm diameter interference filter that has a 3.0 nm bandwidth with a center wavelength of 630.0 nm. The integration time between the two consecutive images is 3 min. For all the images, the effects of compression and curving of the all-sky lens have been moved by an unwarping process (Garcia et al., 1997) and mapped into a uniform geographic coordinate system. The mapping area of the image was from 13.5° to 26° in geographic latitude (GLAT) and from 102.0° to 116.0° in geographic longitude (GLON).

3. Observations and Discussions

3.1. Typical Examples of EPDs Observed by the *Swarm* Lower Pair Satellites Showing Different Structures

Before showing the EPD example coincidently observed by *Swarm* satellites and all-sky imager at Fuke, In Figure 1, we first presented three typical examples of EPDs observed by the Swarm lower pair satellite showing different structures. For each example, the coordinated universal time (UTC), LT, ALT, and GLON when the two satellites passed over the geographic equator have been listed in the topside of the figure. During the three examples, *Swarm* C was 7 s ahead of Swarm A when it flew over the geographic equator and there was also 6 min difference in LT between them due to their 1.4 longitudinal separations. The first example was observed on 14 October 2014, and the in situ electron density observed by *Swarm* A (blue) showed clear depletions between ±9° magnetic latitude (MLAT), while no depletions were seen from *Swarm* C (green). In the second example observed on 20 October 2014, the electron

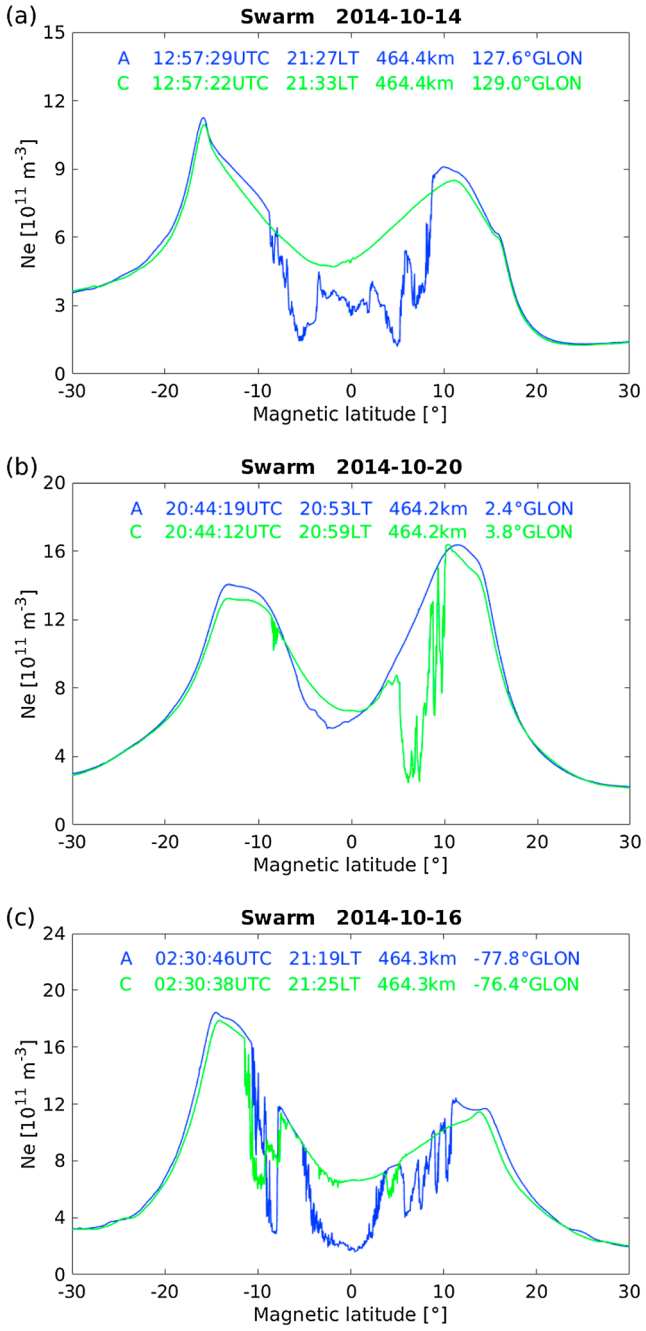

Figure 1. Examples of equatorial plasma depletions (EPDs) observed by the lower pair of *Swarm* satellites: (a) only *Swarm* A observed EPDs, (b) only *Swarm* C observed EPDs, and (c) both *Swarm* A and C observed EPDs, but showing quite different latitudinal structures.

density measured by *Swarm* C showed depletions at both southern (around −8.5° MLAT) and northern (5–10° MLAT) hemispheres, but neither of the depletions were observe by *Swarm* A. During the third example observed on 16 October 2014, both satellites observed electron density depletions, but with obvious differences. For example, the depletions between −5° and 4° MLAT as well as that between 5–11° MLAT only observed by *Swarm* A and around −8° MLAT the density depletions observed by *Swarm* C were found with much lower amplitudes.

3.2. EPD Example Coincidently Observed by *Swarm* Lower Pair Satellites and All-Sky Imager

Figure 2 presented the continuous observation (about 6-h) of airglow images from the all-sky imager at Fuke on the night 23–24 September 2014, during the period from 23:02:10 to 04:44:17 LT. The time difference between two successive images was about 15 min. The location of the Fuke station was marked with a red pentagram, and the LT at the station was provided at the top right for each image. There were some clouds above the station during that night, but from 23:02:10 LT, four distinct EPDs were observed in the airglow images, showing dark bands and marked with "b1," "b2," "b3," and "b4" from eastern to western. The four EPDs were all tilted and elongated from northwest to southeast, with significant longer extension in meridional direction (about 1,000 km) than that in the zonal direction (about 50 km). When compared the consecutive images, the EPDs were found drifting eastward and tilted more westward at later LTs. At 00:02:25 LT, the EPD "b1" was slowly drifted out of the field of view (FOV) of the imager, and another EPD, marked with "b5," entered into the FOV. From 03:01:21 LT, EPDs "b2" and "b3" also slowly drifted out of the FOV, and the EPDs "b4" and "b5" stared to become weak then. From 04:29:09 LT, there were no EPDs observed in the FOV of imager. During the 6-h evolutions, the EPDs were quite active, showing clearly varying structures. For examples, EPDs "b3" and "b4" were found to bifurcate into subbranches from 00:02:38 LT, and from 01:45:35 LT, the subbranches of EPD "b4" were found to merge with each other. We will provide detailed images concerning the bifurcation and merge processes in the later parts.

On the night of 23–24 September 2014, the *Swarm* lower pair satellites flew right over the Fuke station. Among them, *Swarm* C flew over the station at 16:05:39 UTC, corresponding to 23:22:03 LT at the station, while Swarm A was 4 s later and 1.4° westward of *Swarm* C. Figure 3a showed the sequence observations from all-sky imager from 23:20:18 to 23:26:21 LT (the time difference between two images was about 3 min). The four EPDs were seen during this period, and EPD "b2" was almost just above the Fuke station. One interesting feature seen from the airglow images was that around 16° GLAT, the EPDs "b2" and "b3" seemed to connect to each other (see regions within the red dashed rectangle at the frame of 23:23:20 LT). Figure 3b showed the time series of in situ electron density measurements from the lower pair *Swarm* satellites. As the longitude of Swarm C was closer to the station, the UTC, LT, GLAT, GLON, ALT, and LT from the orbital arc of *Swarm* C were listed out at the bottom of the figure. Both satellites observed clear density depletions along their orbital arcs but showed quite different structures. For example, at the northern equatorial ionization anomaly (EIA) crest region, the depletions between 16.6° and 20.4° GLAT were only observed by *Swarm* A, while the *Swarm* C observed large depletions between 10.8° and 16.3° GLAT and *Swarm* A observed depletions between

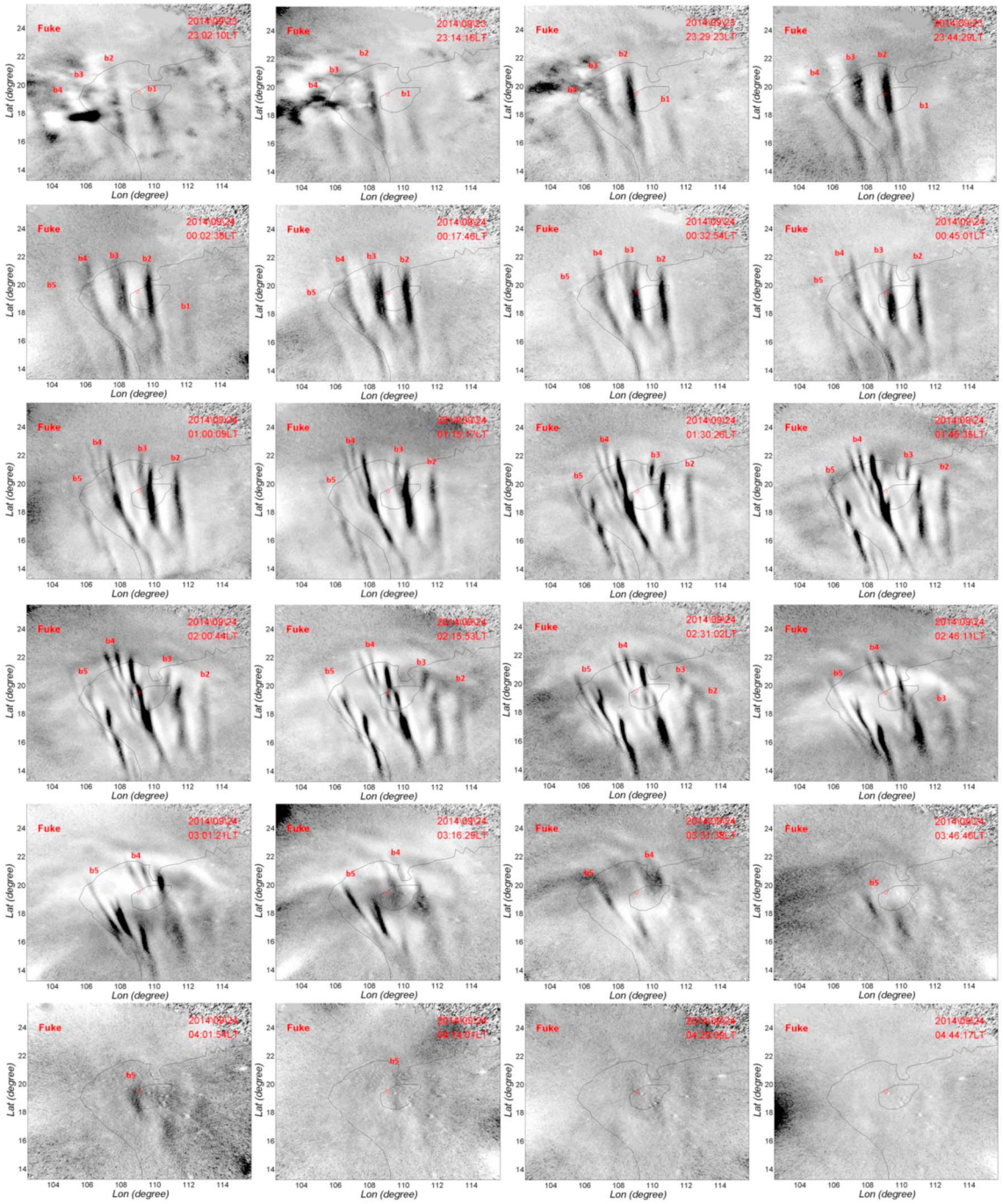

Figure 2. About 6-h (from 23:02:10 to 04:44:17 LT) continuous observations of airglow images from the all-sky imager at Fuke on the night 23–24 September 2014. The time difference between two successive images was about 15 min.

8.3° and 12.9° GLAT. Differences at also the EIA trough and southern hemisphere were founded between the two satellite observations.

Figure 3c showed the orbit arcs of *Swarm* A (blue) and C (green), which have been added to the airglow image observed at 23:23:20 LT (the closest one to the LT when *Swarm* A and C flew over Fuke station). The yellow dashed lines represented the grids of GLAT. Both satellites flew southward with *Swarm* C at longitude of 109.1°E and *Swarm* A at 107.7°E. From the figure we saw that *Swarm* C encountered the EPD of "b2" from about 18° to lower GLAT, while *Swarm* C encountered the EPD "b3" also from about 18° to lower

latitude. The coincidently airglow images seemed agree not so well with the latitudinal profiles of electron density of Swarm satellites, for example, the depletions between 16.6° and 20.4° GLAT observed by *Swarm* A, as it encountered neither "b2" nor "b3" at that latitude. However, we have to point out that the height of the airglow layer seen from the airglow imager was usually assumed to be at a constant ALT, for example, 250 km (Wu et al., 2017), but in fact the 630 nm airglow was resulted from both plasma and neutral phenomena in the whole *F* region ionosphere (Adachi et al., 2010, equations (2)–(4)). Huba et al. (2009) showed that the latitudinal shear of zonal neutral wind can significantly affect the titled angle of EPDs in the horizontal (latitude-longitude) plane (see their Figure 4), and the model proposed by Kil et al. (2009) suggested that the depletion regions of EPDs can be described as a "depletion shell" at the equatorial region from a three-dimensional view. The decreases of the eastward plasma drift and zonal neutral wind with increasing latitudes will cause the depletion region drifting slower at latitude further away from the dip equator and result a westward tilted structure of EPD at the horizontal plane. But, this shear flow of plasma drift and zonal neutral wind existed not only in the horizontal plane (latitude direction) but should also be in the vertical plane (ALT direction). If the vertical shear flow reduces with increasing ALT, it will cause the plasma depletion at higher ALT located at further westward. In this example, the *Swarm* satellite flew at about 464 km, which is higher than the assumed airglow layer (250 km); therefore, it is possible that the depletion region seen at *Swarm* altitude is located further westward than the depletions at 250 km. This hypothesis can also be inferred from the proposed shell structure of EPDs in Figures 3 and 5 of Kil et al. (2009) and Figure 8 of Park et al. (2009). With this assumption, it means that the in situ density depletions between 16.6° and 20.4° GLAT of *Swarm* A corresponded to the dark band of EPD "b2" at higher-latitude part, and the depletion regions between 8.3° and 12.9° GLAT of *Swarm* A corresponded to the lower part of EPD "b2," while the *Swarm* C observed density depletions between 10.8° and 16.3° GLAT corresponded to the lower part of EPD "b3." The airglow images shown in this event confirmed that the structures of neighboring EPDs with typical longitudinal extension of about 50 km were possible to cause the different density depletions observed in the in situ electron density of *Swarm* low pair satellites. The results also suggested that when comparing the airglow images with the satellite in situ measurements, the titled variation of EPDs with ALT also has to be taken into account.

3.3. Bifurcation of EPDs

In fact, the airglow images showed even thinner structures of EPDs with longitudinal extension of about 20–30 km during their later evolution processes. Figure 4 presented the time sequence of airglow images from 00:32:54 to 01:03:11 LT on 24 September 2014, and the time difference between two successive images was about 6 min. At 00:32:54 LT, bifurcations (e.g., Mendillo & Tyler, 1983; Zalesak et al., 1982) were seen at the topside of EPDs "b3" and "b4" (above 19° GLAT). EPD "b3" has been divided into three subbranches, marked with "$b3_1$," "$b3_2$," and "$b3_3$," and EPD "b4" has been divided into two branches "$b4_1$" and "$b4_2$." And at 00:45:01 LT, the EPD "b4" continued to bifurcate, a new subbranch seemed to appear at the location of "$b4_2$," but not totally separated from "$b4_2$" (we marked them as "$b4_{2,3}$"). But 6 min later at 00:57:07 LT, the three subbranches of EPD "b4" were clearly separated from each other, and represented as subdark bands during later LTs (see Figure 2). Meanwhile, clear bifurcation structures were also seen from EPD "b5." These subbranches of EPDs, generated through bifurcation, have really thin longitudinal extension of 20–30 km, which is consistent with numerical model simulations (e.g., Huba & Joyce, 2007; Retterer, 2010; Yokoyama et al., 2015). When looked the evolution of bifurcation for a certain EPD, for example, "b3," we saw that the bifurcation first appeared at the higher-latitude part of EPD, and later, it was also observed at lower-latitude parts. From model simulation, Yokoyama et al. (2015) showed that the bifurcated structures were also first observed at the top of EPD. Considering the EPD extended along depleted fluxtubes, the EPD structures at higher apex-height corresponded well to that at higher-latitude part, which was consistent with the airglow images as shown in our study. The varying shapes of EPDs "b3" and "b4," as well as their subbranches, also suggested that during bifurcation the density structures inside EPD were very turbulent. In the example shown by Yokoyama et al. (2015), the bifurcated parts even pinched off from the main structure of EPD, but from the airglow images shown here, we saw that, although the higher-latitude parts of EPDs bifurcated, they still connected together at the lower-latitude part. As pointed out in Figure 3a that the EPDs "b2" and "b3" connect to each other at the lower part, we could further image that these two EPDs may also generated through bifurcation at earlier LT, although we cannot provide direct evidence here; and the bifurcated branches, "b2" and "b3," kept growing and bifurcated again into even thinner structures at later LT.

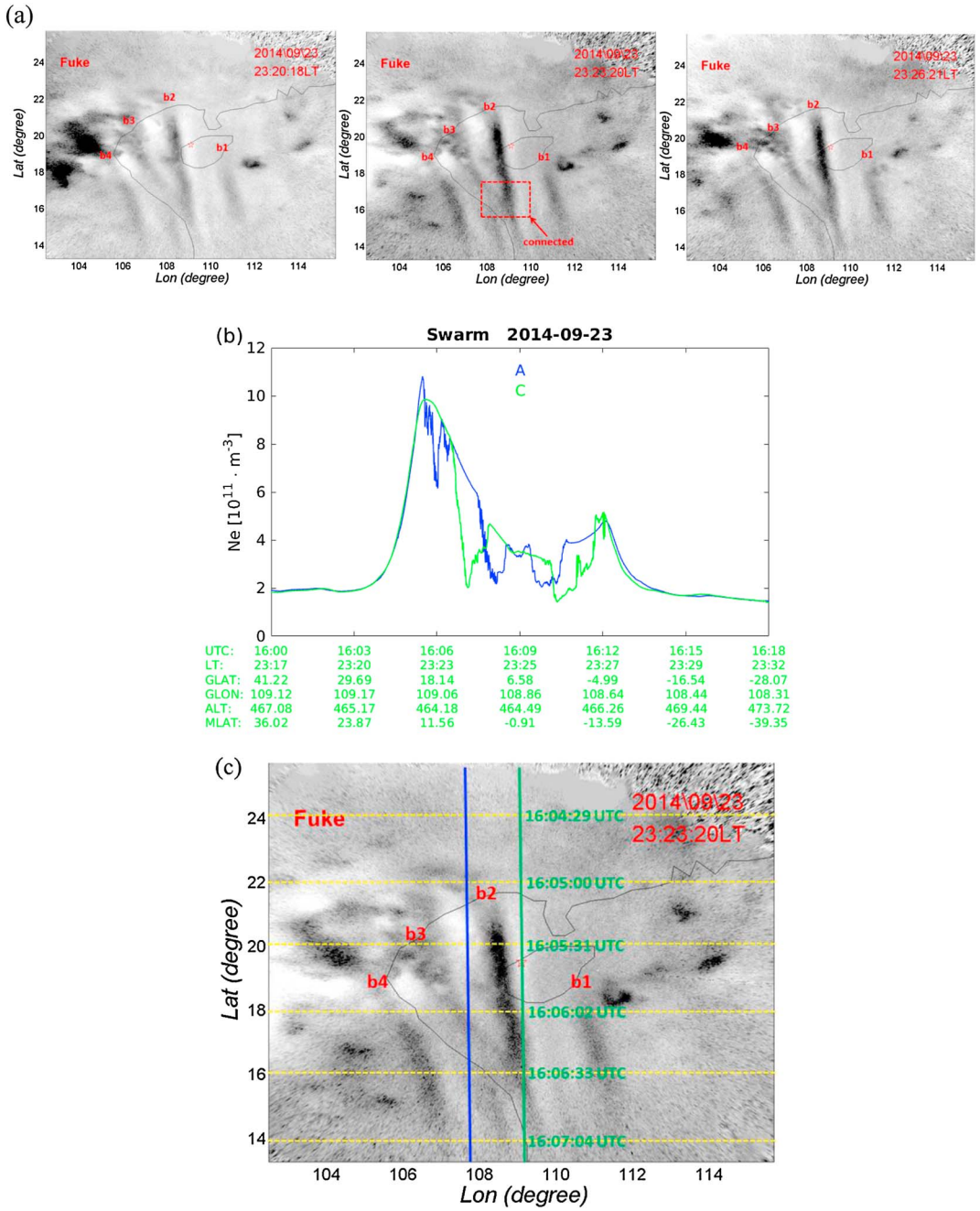

Figure 3. (a) Three successive airglow images with 3 min in time difference from 23:20:18 to 23:26:21 LT on 23 September 2014. During this time the Swarm A and C flew over the Fuke station. (b) The time series of in situ electron density measurements from *Swarm* A (blue) and C (green) satellites. (c) The orbit arcs of *Swarm* A (blue) and C (green) added to the airglow image observed at 23:23:20 LT.

3.4. Merging of EPDs

As shown in Figure 2, the subbranches of EPDs were still active after bifurcation. Figure 5 presented the time sequence of airglow images from 02:00:44 to 02:15:53 LT on 24 September 2014, and the time difference between two successive images was about 3 min. At 02:00:44 LT, the subbranch of EPD "$b4_2$" starts to merge with "$b4_1$." The region marked with a red-dashed rectangle in each image indicated where merging observed. At 02:15:53 LT, the three subbranches of EPD "b_4" merged with each other, forming a really complicated mesh of depleted regions. By model simulation, Huba et al. (2015) explained that during the

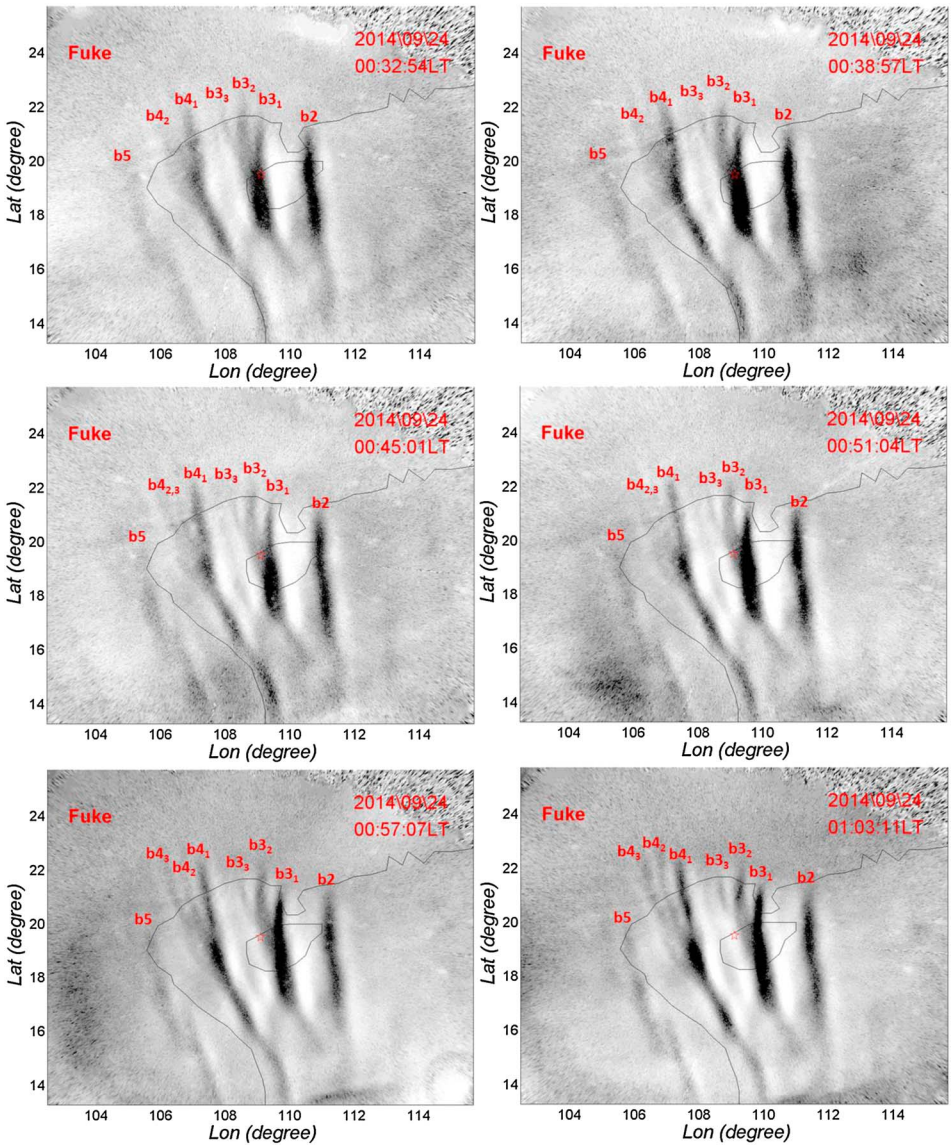

Figure 4. The time sequence of airglow images from 00:32:54 to 01:03:11 LT on 24 September 2014, showing the bifurcation process of EPDs. The time difference between two successive images was about 6 min.

developing of EPDs, the electrostatic potential associated with one EPD can connect with that of a neighboring EPD, which provided a pathway for the low-density plasma in one EPD to flow into the adjoining EPD and merge with it. With observations from all-sky imager, Narayanan et al. (2016) also pointed out that three potential ways may exist in the merging of EPD: (a) One of the EPDs tilts and reaches the location of the adjacent growing EPD finally merging with it; (b) some of the branches of an EPB arising from secondary instabilities reach out to adjacent EPD and merge with it; and (c) the eastward zonal drift of the EPB on the eastern side slows down while the adjacent EPB on the western side drifts relatively faster and catches up. Our result shown here suggested that the subbranches generated from one same EPD can also merge with each other and finally formed a really complicated mesh of depleted regions. Another interesting feature we want to point it out here was that the EPDs "b4" and "b5" were separated by only about 2° in longitude (about 220 km); therefore, they were expected to share the same background ionospheric and neutral conditions. However, the bifurcations were seen from both EPDs, while the merging of the subbranches was only observed between the subbranches of EPD "b4." This result also suggested that besides the background ionospheric and

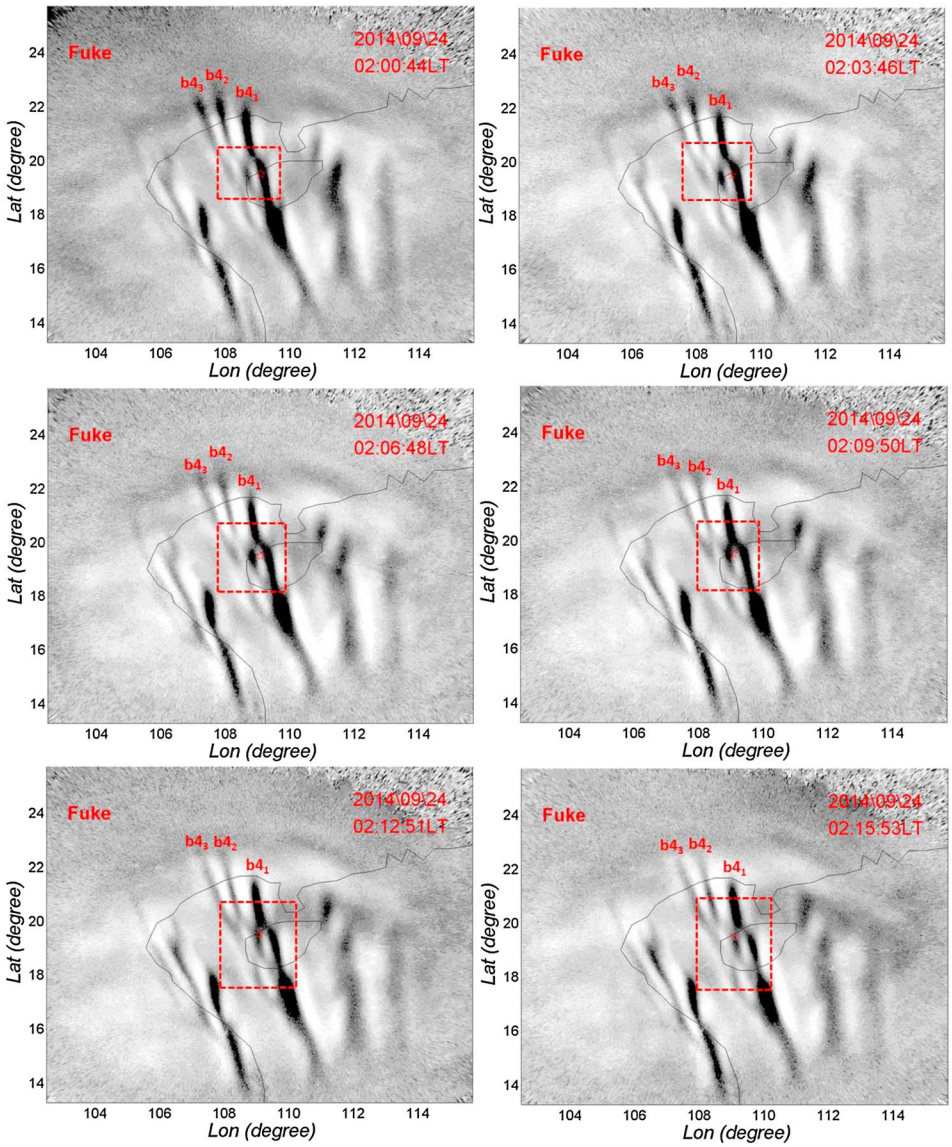

Figure 5. The time sequence of airglow images from 02:00:44 to 02:15:53 LT on 24 September 2014, showing the merging process between the subbranches of bifurcated EPDs. The time difference between two successive images was about 6 min.

neutral conditions, the plasma turbulences inside the depleted regions are also important for causing different evolutions of EPDs during their development.

4. Summary

In this study we provided an example of EPD that coincidently observed by the *Swarm* lower pair satellite and an all-sky imager located at south China, and the findings can be summarized as follows:

1. The EPDs observed by all-sky imager showed structures elongated tilted from northwest to southeast direction, with longitudinal extension of about 50 km. This kind of longitudinal thin structures of neighboring EPDs generally explained well the differences of in situ electron density depletions simultaneously observed by the *Swarm* low pair satellites.
2. Our results also suggested that when comparing the in situ observation of EPDs from satellites with airglow images, the vertical structure of EPDs should also be taken into account.

3. The EPDs during postmidnight hours were not only the dead or fossil EPDs. Instead, they were quite active and showed both bifurcation and merging processes.
4. The bifurcation was first observed at the higher-latitude part of EPD, and then observed at lower latitudes. The subbranches of EPD generated through bifurcation showed even thinner longitudinal extension of about 20–30 km, and later the subbranches started to merge with each other, forming a really complicated mesh of deleted regions.

Acknowledgments
The European Space Agency (ESA) is acknowledged for providing the *Swarm* data. The official *Swarm* website is http://earth.esa.int/Swarm, and the server for *Swarm* data distribution is ftp://Swarm-diss.eo.esa.int. Chao Xiong is partly supported by the Priority Program 1788 "Dynamic Earth" of the German Research Foundation (DFG). The work of Jiyao Xu, Kun Wu, and Wei Yuan are supported by the National Natural Science Foundation of China (41674152 and 41331069) and The Chinese Meridian Project. The airglow data used in this study may be obtained by contacting the authors.

References

Adachi, T., Yamaoka, M., Yamamoto, M., Otsuka, Y., Liu, H., Hsiao, C.-C., et al. (2010). Midnight latitude-altitude distribution of 630 nm airglow in the Asian sector measured with FORMOSAT-2/ISUAL. *Journal of Geophysical Research*, *115*, A09315. https://doi.org/10.1029/2009JA015147

Booker, H. G., & Wells, H. W. (1938). Scattering of radio waves by the F-region of the ionosphere. *Journal of Geophysical Research*, *43*(3), 249–256. https://doi.org/10.1029/TE043i003p00249

Burke, W. J., Gentile, L. C., Huang, C. Y., Valladares, C. E., & Su, S. Y. (2004). Longitudinal variability of equatorial plasma bubbles observed by DMSP and ROCSAT-1. *Journal of Geophysical Research*, *109*, A12301. https://doi.org/10.1029/2004JA010583

Garcia, F. J., Taylor, M. J., & Kelley, M. C. (1997). Two-dimensional spectral analysis of mesospheric airglow image data. *Applied Optics*, *36*(29), 7374–7385. https://doi.org/10.1364/AO.36.007374

Huang, C.-S., de La Beaujardiere, O., Roddy, P. A., Hunton, D. E., Liu, J. Y., & Chen, S. P. (2014). Occurrence probability and amplitude of equatorial ionospheric irregularities associated with plasma bubbles during low and moderate solar activities (2008–2012). *Journal of Geophysical Research: Space Physics*, *119*, 1186–1199. https://doi.org/10.1002/2013JA019212

Huba, J. D., & Joyce, G. (2007). Equatorial spread F modeling: Multiple bifurcated structures, secondary instabilities, large density 'bite-outs,' and supersonic flows. *Geophysical Research Letters*, *34*, L07105. https://doi.org/10.1029/2006GL028519

Huba, J. D., Ossakow, S. L., Joyce, G., Krall, J., & England, S. L. (2009). Three-dimensional equatorial spread F modeling: Zonal neutral wind effects. *Geophysical Research Letters*, *36*, L19106. https://doi.org/10.1029/2009GL040284

Huba, J. D., Wu, T.-W., & Makela, J. J. (2015). Electrostatic reconnection in the ionosphere. *Geophysical Research Letters*, *42*, 1626–1631. https://doi.org/10.1002/2015GL063187

Hysell, D. L., & Seyler, C. E. (1998). A renormalization group approach to estimation of anomalous diffusion in the unstable equatorial F region. *Journal of Geophysical Research*, *103*(A11), 26,731–26,737. https://doi.org/10.1029/98JA02616

Kelley, M. C. (2009). *The Earth's Ionosphere: Electrodynamics and Plasma Physics* (2nd ed.). New York: Elsevier.

Kelley, M. C., Haerendel, G., Kappler, G. H., Valenzuela, A., Balsley, B. B., Carter, D. A., et al. (1976). Evidence for a Rayleigh-Taylor type instability and upwelling of depleted density regions during equatorial spread F. *Geophysical Research Letters*, *3*(8), 448–450. https://doi.org/10.1029/GL003i008p00448

Kil, H., Heelis, R. A., Paxton, L. J., & Oh, S.-J. (2009). Formation of a plasma depletion shell in the equatorial ionosphere. *Journal of Geophysical Research*, *114*, A11302. https://doi.org/10.1029/2009JA014369

Kil, H., Su, S.-Y., Paxton, L. J., Wolven, B. C., Zhang, Y., Morrison, D., & Yeh, H. C. (2004). Coincident equatorial bubble detection by TIMED/GUVI and ROCSAT-1. *Geophysical Research Letters*, *31*, L03809. https://doi.org/10.1029/2003GL018696

Lühr, H., Xiong, C., Park, J., & Rauberg, J. (2014). Systematic study of intermediate-scale structures of equatorial plasma irregularities in the ionosphere based on CHAMP observations. *Frontiers of Physics*, *2*, 15. https://doi.org/10.3389/fphy.2014.00015

Mendillo, M., & Tyler, A. (1983). Geometry of depleted plasma regions in the equatorial ionosphere. *Journal of Geophysical Research*, *88*(A7), 5778–5782. https://doi.org/10.1029/JA088iA07p05778

Mukherjee, G. K., Carlo, L., Mahajan, S. H., & Patil, P. T. (1998). First results of all-sky imaging from India. *Earth, Planets and Space*, *50*(2), 119–127. https://doi.org/10.1186/BF03352093

Narayanan, V. L., Gurubaran, S., & Shiokawa, K. (2016). Direct observational evidence for the merging of equatorial plasma bubbles. *Journal of Geophysical Research: Space Physics*, *121*, 7923–7931. https://doi.org/10.1002/2016JA022861

Park, J., Lühr, H., Stolle, C., Rother, M., Min, K. W., & Michaelis, I. (2009). The characteristics of field-aligned currents associated with equatorial plasma bubbles as observed by the CHAMP satellite. *Annales de Geophysique*, *27*(7), 2685–2697. https://doi.org/10.5194/angeo-27-2685-2009

Pimenta, A. A., Bittencourt, J. A., Fagundes, P. R., Sahai, Y., Buriti, R. A., Takahashi, H., & Taylor, M. J. (2003). Ionospheric plasma bubble zonal drifts over the tropical region: A study using OI 630 nm emission all-sky images. *Journal of Atmospheric and Solar: Terrestrial Physics*, *65*(10), 1117–1126. https://doi.org/10.1016/S1364-6826(03)00149-4

Retterer, J. M. (2010). Forecasting low-latitude radio scintillation with 3-D ionospheric plume models: 1. Plume model. *Journal of Geophysical Research*, *115*, A03306. https://doi.org/10.1029/2008JA013839

Stolle, C., Lühr, H., Rother, M., & Balasis, G. (2006). Magnetic signatures of equatorial spread F as observed by the CHAMP satellite. *Journal of Geophysical Research*, *111*, A02304. https://doi.org/10.1029/2005JA011184

Su, S.-Y., Liu, C. H., Ho, H. H., & Chao, C. K. (2006). Distribution characteristics of topside ionospheric density irregularities: Equatorial versus midlatitude regions. *Journal of Geophysical Research*, *111*, A06305. https://doi.org/10.1029/2005JA011330

Su, S.-Y., Yeh, H. C., & Heelis, R. A. (2001). ROCSAT 1 ionospheric plasma and electrodynamics instrument observations of equatorial spread F: An early transitional scale result. *Journal of Geophysical Research*, *106*(A12), 29,153–29,159. https://doi.org/10.1029/2001JA900109

Tsunoda, R. T. (1980). Magnetic-field-aligned characteristics of plasma bubbles in the nighttime equatorial ionosphere. *Journal of Atmospheric and Terrestrial Physics*, *42*(8), 743–752. https://doi.org/10.1016/0021-9169(80)90057-4

Weber, E. J., Buchau, J., Eather, R. H., & Mende, S. B. (1978). North-south aligned equatorial airglow depletions. *Journal of Geophysical Research*, *83*(A2), 712–716. https://doi.org/10.1029/JA083iA02p00712

Wu, K., Xu, J., Wang, W., Sun, L., Liu, X., & Yuan, W. (2017). Interesting equatorial plasma bubbles observed by all-sky imagers in the equatorial region of China. *Journal of Geophysical Research: Space Physics*, *122*, 10,596–10,611. https://doi.org/10.1002/2017JA024561

Xiong, C., Park, J., Lühr, H., Stolle, C., & Ma, S. Y. (2010). Comparing plasma bubble occurrence rates at CHAMP and GRACE altitudes during high and low solar activity. *Annales de Geophysique*, *28*, 1647–1658. https://doi.org/10.5194/angeo-28-1647-2010

Xiong, C., Stolle, C., & Lühr, H. (2016). The *Swarm* satellite loss of GPS signal and its relation to ionospheric plasma irregularities. *Space Weather*, *14*, 563–577. https://doi.org/10.1002/2016SW001439

Xiong, C., Stolle, C., Lühr, H., Park, J., Fejer, B. G., & Kervalishvili, G. N. (2016). Scale analysis of the equatorial plasma irregularities derived from *Swarm* constellation. *Earth, Planets and Space*, *68*(1). https://doi.org/10.1186/s40623-016-0502-5

Yokoyama, T., Shinagawa, H., & Jin, H. (2015). Nonlinear growth, bifurcation and pinching of equatorial plasma bubble simulated by three-dimensional high-resolution bubble model. *Journal of Geophysical Research: Space Physics*, *119*, 10,474–10,482. https://doi.org/10.1002/2014JA020708

Zalesak, S. T., Ossakow, S. L., & Chaturvedi, P. K. (1982). Nonlinear equatorial spread F: The effect of neutral winds and background Pedersen conductivity. *Journal of Geophysical Research*, *87*(A1), 151–166. https://doi.org/10.1029/JA087iA01p00151